

Optimal Transport for Time-Varying Multi-Agent Coverage Control

Italo Napolitano^a, Mario di Bernardo^{*, b}

^a*Modeling and Engineering Risk and Complexity, Scuola Superiore Meridionale, Naples, Italy*

^b*Department of Electrical Engineering and Information Technology, University of Naples Federico II and Modeling and Engineering Risk and Complexity, Scuola Superiore Meridionale, Naples, Italy*

Abstract

Coverage control algorithms have traditionally focused on static target densities, where agents are deployed to optimally cover a fixed spatial distribution. However, many applications involve time-varying densities, including environmental monitoring, surveillance, and adaptive sensor deployment. Although time-varying coverage strategies have been studied within Voronoi-based frameworks, recent works have reformulated static coverage control as a semi-discrete optimal transport problem. Extending this optimal transport perspective to time-varying scenarios has remained an open challenge. This paper presents a rigorous optimal transport formulation for time-varying coverage control, in which agents minimize the instantaneous Wasserstein distance to a continuously evolving target density. The proposed solution relies on a coupled system of differential equations governing agent positions and the dual variables that define Laguerre regions. In one-dimensional domains, the resulting system admits a closed-form analytical solution, offering both computational benefits and theoretical insight into the structure of optimal time-varying coverage. Numerical simulations demonstrate improved tracking performance compared to quasi-static and Voronoi-based methods, validating the proposed framework.

Key words: Optimal Transport; Multi-Agent Systems; Coverage Control; Wasserstein Distance; Time-Varying Density; Autonomous Systems;

1 Introduction

Coverage control addresses the coordination of mobile agents to achieve an optimal spatial distribution over a domain for sensing or monitoring. This class of problems has received extensive attention over the past two decades [25,13,24,30]. The seminal work of Cortés et al. [13] introduced a framework based on Centroidal Voronoi Tessellations (CVTs), in which agents move toward the centroids of their Voronoi regions to minimize a locational cost. This gradient-based strategy has proven highly effective for static target densities and admits convergence guarantees to locally optimal configurations [8].

In many scenarios, however, agents must track time-varying densities. Representative examples of scenarios

requiring coverage of densities that evolve in time include environmental monitoring of dynamic phenomena, surveillance of moving crowds, adaptive sensor deployment under changing conditions, and the tracking of probability distributions in stochastic systems, with applications to leader-follower, predator-prey, environmental monitoring, and phoretic interaction scenarios [30]. Allowing the target density to vary in time also leads naturally to a formulation of formation control in probability space [4].

Extending static coverage to this setting remains challenging. Lee et al. [27] proposed control laws incorporating temporal derivatives to compensate for density evolution, while Lin et al. [30] employed a time-varying Control Lyapunov Function; both approaches operate within the Voronoi-based framework. Although effective, Voronoi-based methods do not enforce equal-mass partitions, which limits the accuracy of the approximation when the goal is to match a target distribution.

Optimal transport provides an alternative perspective by offering a principled means of comparing contin-

* This paper was not presented at any IFAC meeting. * Corresponding author: M. di Bernardo

Email addresses: i.napolitano@ssmeridionale.it (Italo Napolitano), mario.dibernardo@unina.it (Mario di Bernardo*).

uous and discrete measures through the Wasserstein distance [40]. In particular, the semi-discrete formulation defines Wasserstein distances between a continuous measure and a discrete set of points, making it well suited for coverage control [25,26,22]. Inoue et al. [22] cast static coverage as a semi-discrete optimal transport problem using Laguerre diagrams and the Kantorovich dual formulation, establishing connections between CVT methods and optimal transport. Krishnan and Martinez [26] developed distributed algorithms with convergence guarantees, but mostly focused on large-scale limits. Both works restricted attention to static densities.

This paper addresses this challenge by developing an optimal transport framework for time-varying coverage control. The problem is formulated as a continuous-time semi-discrete optimal transport task in which agents minimize, at each instant, the Wasserstein distance between their empirical measure and a time-varying target measure. Unlike gradient-based extensions of CVT [27], the proposed formulation is grounded in the optimal transport framework, enforcing equal-mass regions and yielding a more accurate approximation of the target density. Differently from static optimal transport approaches [22], instead, we explicitly account for the continuous temporal evolution of the target measure. Numerical simulations demonstrate superior tracking performance compared to both quasi-static optimal transport and Voronoi-based methods. To the best of the authors' knowledge, this is the first optimal transport solution to time-varying coverage control.

The main contributions can be summarized as follows. First, time-varying coverage is formulated as a time-dependent semi-discrete optimal transport problem. Second, coupled dynamics for agents and dual variables are derived, combining proportional feedback with feed-forward compensation to achieve exponential tracking of the time-varying Laguerre barycenters. Third, for one-dimensional domains, relevant to, e.g., line formation control, coastal monitoring, and pipeline inspection, the feedforward term is computed analytically, yielding explicit dynamics.

The paper is organized as follows. Section 2 reviews semi-discrete optimal transport and its connection to coverage control. Section 3 formulates the time-varying coverage problem. Section 4 derives the proposed control law. Section 5 presents the one-dimensional case. Section 6 provides numerical validation, and Section 7 concludes the paper.

1.1 Notation

Let $\Omega \subset \mathbb{R}^d$ be a compact convex domain. Scalars are lowercase (x), vectors bold lowercase (\mathbf{x}), and matrices bold uppercase (\mathbf{A}). The operator $\text{vec}(\cdot)$ stacks vectors,

e.g., $\mathbf{p} := \text{vec}(\mathbf{p}_1, \dots, \mathbf{p}_N)$. Time and spatial derivatives are ∂_t and $\partial_{\mathbf{x}}$, respectively. Standard notation for norms, gradients, and Hessians follows [8].

We denote $\mathcal{P}_2(\Omega)$ as the set of Borel probability measures on Ω with finite second moment. Target quantities carry a bar, e.g., the target density $\bar{\rho}(\mathbf{x}, t) : \Omega \times \mathbb{R}_{\geq 0} \rightarrow \mathbb{R}_{\geq 0}$ induces the absolutely continuous measure $\bar{\mu}_t \in \mathcal{P}_2(\Omega)$, i.e., $d\bar{\mu}(\mathbf{x}) = \bar{\rho}(\mathbf{x})d\mathbf{x}$. Agent i is located at $\mathbf{p}_i(t) \in \Omega$, and the ensemble defines the empirical measure $\mu_t := \frac{1}{N} \sum_{i=1}^N \delta_{\mathbf{p}_i(t)}$. The p -Wasserstein distance is $\mathcal{W}_p(\cdot, \cdot)$. The Laguerre cell of agent i is \mathcal{V}_i , with mass $a_i(t)$ and barycenter $\mathbf{b}_i(t)$; Voronoi counterparts carry a tilde ($\tilde{\mathcal{V}}_i$).

2 Background

2.1 Semi-Discrete Optimal Transport

Optimal transport provides a principled framework for comparing probability measures by minimizing the cost of redistributing mass from a distribution to the other [40]. The Kantorovich formulation [23] relaxes Monge's deterministic transport problem [34] by allowing probabilistic transport plans. Given probability measures μ and $\bar{\mu}$ on \mathcal{X} and \mathcal{Y} and a cost $c : \mathcal{X} \times \mathcal{Y} \rightarrow \mathbb{R}$, the Kantorovich problem is

$$\min_{\pi \in \Pi(\mu, \bar{\mu})} \int_{\mathcal{X} \times \mathcal{Y}} c(x, y) d\pi(x, y)$$

where $\Pi(\mu, \bar{\mu})$ denotes the set of couplings with marginals μ and $\bar{\mu}$. This convex relaxation admits strong duality under mild assumptions [40]. For $c(x, y)$ being the quadratic cost on \mathbb{R}^d , the 2-Wasserstein distance squared is defined as

$$\mathcal{W}_2^2(\mu, \bar{\mu}) := \min_{\pi \in \Pi(\mu, \bar{\mu})} \int_{\mathbb{R}^d \times \mathbb{R}^d} \frac{1}{2} \|\mathbf{x} - \mathbf{y}\|_2^2 d\pi(\mathbf{x}, \mathbf{y}),$$

where the objective function is known as *Kantorovich cost*.

Then, the dual Kantorovich problem reads

$$\begin{aligned} \max_{(\phi, \psi)} \quad & C_K := \int_{\mathbb{R}^d} \phi(\mathbf{x}) d\mu(\mathbf{x}) + \int_{\mathbb{R}^d} \psi(\mathbf{y}) d\bar{\mu}(\mathbf{y}) \\ \text{s.t.} \quad & \phi(\mathbf{x}) + \psi(\mathbf{y}) \leq \frac{1}{2} \|\mathbf{x} - \mathbf{y}\|_2^2, \quad \forall (\mathbf{x}, \mathbf{y}) \in \mathbb{R}^d \times \mathbb{R}^d. \end{aligned}$$

Moreover, the optimal potentials satisfy the c -transform

$$\psi^*(\mathbf{y}) = \inf_{\mathbf{x} \in \mathbb{R}^d} \left(\frac{1}{2} \|\mathbf{x} - \mathbf{y}\|_2^2 - \phi^*(\mathbf{x}) \right),$$

allowing the dual problem to be expressed solely in terms of ϕ^* , which is particularly convenient in semi-discrete settings.

In the semi-discrete setting, one compares a discrete measure against a continuous one, a scenario where standard divergences and distances are undefined [35,39,1]. Here, the optimal transport induces a partition of the domain into Laguerre cells, generalizing Voronoi cells through additive weights [18,2,35].

Consider a discrete probability measure $\mu := \frac{1}{N} \sum_{i=1}^N \delta_{\mathbf{p}_i}$ with $\mathbf{p}_i \in \Omega$, and an absolutely continuous measure $\bar{\mu}$ on Ω with density $\bar{\rho}(\mathbf{x})$. For the squared Euclidean cost, the Kantorovich dual formulation yields [40,35]

$$\mathcal{W}_2^2(\mu, \bar{\mu}) = \max_{\phi \in \mathbb{R}^N} F(\mathbf{p}, \phi),$$

where $\phi = \text{vec}(\phi_1, \dots, \phi_N)$ collects the dual variables and

$$F(\mathbf{p}, \phi) := \sum_{i=1}^N \left[\int_{\mathcal{V}_i(\mathbf{p}, \phi)} \frac{1}{2} \|\mathbf{p}_i - \mathbf{x}\|_2^2 \bar{\rho}(\mathbf{x}) d\mathbf{x} + \left(\frac{1}{N} - \int_{\mathcal{V}_i(\mathbf{p}, \phi)} \bar{\rho}(\mathbf{x}) d\mathbf{x} \right) \phi_i \right]. \quad (1)$$

The i -th Laguerre cell is defined as

$$\mathcal{V}_i(\mathbf{p}, \phi) := \left\{ \mathbf{x} \in \Omega : \frac{1}{2} \|\mathbf{p}_i - \mathbf{x}\|_2^2 - \phi_i \leq \frac{1}{2} \|\mathbf{p}_j - \mathbf{x}\|_2^2 - \phi_j, \forall j \neq i \right\}. \quad (2)$$

Laguerre cells generalize Voronoi cells through additive weights [18,2,35]; when $\phi_i = 0$ for all i , they reduce to the standard Voronoi partition. Notably, the function F is concave in ϕ [3] and, in this setting, the dual variable ϕ is a vector of cardinality N thanks to the semi-discrete nature of the problem, which greatly simplifies its tractability.

The mass and barycenter of each Laguerre cell,

$$a_i := \int_{\mathcal{V}_i} \bar{\rho}(\mathbf{x}) d\mathbf{x}, \quad \mathbf{b}_i := \frac{1}{a_i} \int_{\mathcal{V}_i} \mathbf{x} \bar{\rho}(\mathbf{x}) d\mathbf{x}, \quad (3)$$

play a central role in optimal transport-based coverage algorithms.

2.2 Coverage Control

Coverage control addresses how to optimally position mobile agents over a domain weighted by a target density [8,38,37,20]. The seminal work of Cortés et al. [13] introduced a Voronoi-based framework in which agents move toward the centroids of their Voronoi regions to minimize a locational cost. Extensions to time-varying densities were developed in [12,28], employing feedback and feed-forward structures to track moving Voronoi barycenters, or exploiting Control Lyapunov Functions [30].

Inoue et al. [22] reformulated static coverage as a semi-discrete optimal transport problem, recasting the objective as

$$\min_{\mathbf{p}} \max_{\phi} F(\mathbf{p}, \phi), \quad (4)$$

with F defined in (1). The associated gradient ascent-descent dynamics are

$$\dot{\mathbf{p}}_i(t) = -K_x(\mathbf{p}_i(t) - \mathbf{b}_i(t)), \quad (5)$$

$$\dot{\phi}_i(t) = K_\phi \left(\frac{1}{N} - a_i(t) \right), \quad (6)$$

which drive the system toward the saddle point $\mathbf{p}^* = \mathbf{b}^*$ with $a_i = \frac{1}{N}$ for all i . At optimality, the agents partition the domain into equal-mass regions and coincide with their respective Laguerre barycenters.

Unlike Voronoi-based methods, the optimal transport formulation enforces equal-mass regions, which yields a more accurate approximation of the target density.

When $\phi_i(t) = \phi$ for all i and all t , Laguerre regions reduce to Voronoi partitions (see Remark 4). The optimal transport formulation yields equal-mass regions, improving density approximation. Figure 1 illustrates the difference between Voronoi and Laguerre regions for five agents tasked with covering a Gaussian target distribution in a one-dimensional domain. The Voronoi-based agents are more evenly spaced, whereas the Laguerre-based agents cluster around the peak of the Gaussian, thereby providing a closer approximation of the target distribution.

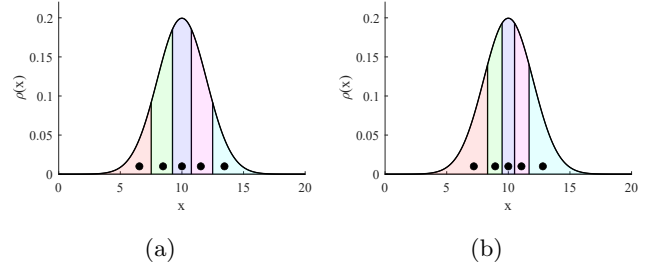


Fig. 1. Difference between (a) Voronoi and (b) Laguerre regions (colored areas) when 5 samples (black dots) approximate the same Gaussian distribution (solid black line).

However, the approach of Inoue et al. [22] is restricted to stationary distributions. The present work extends this framework to time-varying target densities.

3 Modeling and Problem Statement

Consider a compact convex domain $\Omega \subseteq \mathbb{R}^d$, and let $\bar{\rho}(\mathbf{x}, t) : \Omega \times \mathbb{R}_{\geq 0} \rightarrow \mathbb{R}_{\geq 0}$ denote a possibly time-varying target density function. The absolutely continuous target measure $\bar{\mu}_t \in \mathcal{P}_2(\Omega)$ is induced by $\bar{\rho}(\mathbf{x}, t)$.

Assumption 1 $\bar{\rho}(\mathbf{x}, t)$ is C^1 and Lipschitz in time.

The i -th controlled agent is located at position $\mathbf{p}_i(t) \in \Omega$ at time t , and collect the positions of all N agents in the vector $\mathbf{p}(t) := \text{vec}(\mathbf{p}_1(t), \dots, \mathbf{p}_N(t)) \in \Omega^N$. Each agent is fully actuated and evolves according to:

$$\dot{\mathbf{p}}_i(t) = \mathbf{u}_i(t), \quad \text{for } i = 1, \dots, N, \quad (7)$$

where $\mathbf{u}_i(t) \in \mathbb{R}^d$ is the control input driving the i -th agent. The empirical measure of the agents at time t , denoted by μ_t , is defined as the normalized sum of Dirac delta measures centered at the agent positions:

$$\mu_t := \frac{1}{N} \sum_{i=1}^N \delta_{\mathbf{p}_i(t)}. \quad (8)$$

Assumption 2 Agents never overlap, i.e., $\mathbf{p}_i(t) \neq \mathbf{p}_j(t) \forall (i, j), \forall t > 0$.

This assumption is standard for this class of problems [12,22] and can be enforced by incorporating short-range repulsion terms for collision avoidance in (7).

The objective is to design a control law that computes $\mathbf{u}_i(t)$ for $i = 1, \dots, N$, so that, at each time t , the positions of the agents minimize the mismatch between the desired distribution and the empirical distribution, i.e.,

$$\min_{\mathbf{p}(t) \in \Omega^N} \mathcal{W}_2^2(\mu_t, \bar{\mu}_t). \quad (9)$$

Notice that this formulation corresponds to a semi-discrete optimal transport problem, a setting similar to the one in [22] and detailed in Sec. 2.2, but considering a time-varying target density instead of a stationary one.

Remark 1 The present work aims at instantaneous Wasserstein minimization, which is fundamentally different from dynamic optimal transport in the Benamou-Brenier formulation [5]. Whereas the latter seeks geodesics in the space of probability measures by jointly optimizing mass trajectories over an entire time horizon, the approach proposed here minimizes the transport cost at each instant independently in a semi-discrete setting.

4 Time-varying Optimal Transport Strategy

Consider the Laguerre regions $\mathcal{V}_i = \mathcal{V}_i(\mathbf{p}(t), \phi(t))$ for $i = 1, \dots, N$ defined in (2) and detailed in Sec. 2.2. The concepts of mass and barycenter extend naturally to the time-varying setting:

$$a_i(t) := \int_{\mathcal{V}_i} \bar{\rho}(\mathbf{x}, t) d\mathbf{x}, \quad \mathbf{b}_i(t) := \frac{1}{a_i(t)} \int_{\mathcal{V}_i} \mathbf{x} \bar{\rho}(\mathbf{x}, t) d\mathbf{x}.$$

As in [22], the Kantorovich dual formulation can be exploited to rewrite the objective function of (9) in a form that explicitly captures the time dependency of the target distribution:

$$\mathcal{W}_2^2(\mu_t, \bar{\mu}_t) = \max_{\phi(t)} F(\mathbf{p}(t), \phi(t), t), \quad (10)$$

where

$$F := \sum_{i=1}^N \left[\int_{\mathcal{V}_i(\mathbf{p}(t), \phi(t))} \frac{1}{2} \|\mathbf{p}_i(t) - \mathbf{x}\|_2^2 \bar{\rho}(\mathbf{x}, t) d\mathbf{x} \right. \\ \left. + \left(\frac{1}{N} - \int_{\mathcal{V}_i(\mathbf{p}(t), \phi(t))} \bar{\rho}(\mathbf{x}, t) d\mathbf{x} \right) \phi_i(t) \right]. \quad (11)$$

Accordingly, (9) can be recast as a min-max problem with explicit time dependence:

$$\min_{\mathbf{p}(t)} \max_{\phi(t)} F(\mathbf{p}(t), \phi(t), t). \quad (12)$$

4.1 Proposed solution

To track a local saddle point of the instantaneous dual problem, and thereby achieve local minimization of the Wasserstein distance, dynamics in continuous time are proposed for both the agent positions $\mathbf{p}(t)$ and the dual variables $\phi(t)$. It is assumed that an estimate of $\partial_t \bar{\rho}(\mathbf{x}, t)$ is available, enabling exponential tracking of the optimum as it evolves.

Theorem 1 Suppose Assumptions 1 and 2 hold. The following continuous-time dynamics for the agent positions $\mathbf{p}_i(t)$ and the dual variables $\phi(t)$ achieve local saddle-point tracking for Problem (9):

$$\begin{cases} \dot{\mathbf{p}}_i(t) = -K_x(\mathbf{p}_i(t) - \mathbf{b}_i(t)) + \dot{\mathbf{b}}_i(t), \\ \dot{\phi}_i(t) = K_\phi \left(\frac{1}{N} - a_i(t) \right), \end{cases} \quad (13)$$

for $i = 1, \dots, N$, where $K_x, K_\phi > 0$ are the primal and dual gains, respectively, and $\mathbf{p}(0) = \mathbf{p}_0, \phi(0) = \phi_0$ are arbitrary initial conditions.

Proof. Under the regularity conditions of Assumption 1, the objective function (11) is continuously differentiable with respect to (\mathbf{p}, ϕ) [12,7,32], and gradient-based methods can therefore be applied, as in [22,8].

The partial derivatives of (11) are given by

$$\frac{\partial F}{\partial \mathbf{p}_i} = a_i(t)(\mathbf{p}_i(t) - \mathbf{b}_i(t)), \quad \frac{\partial F}{\partial \phi_i} = \frac{1}{N} - a_i(t). \quad (14)$$

These expressions, as typically found in the literature [7,22], are obtained by applying the Reynolds transport theorem to account for the dependence of the time-varying Laguerre cells on the optimization variables. Boundary terms cancel out because adjacent Laguerre cells share boundaries with opposite normals and the cost is continuous across cells.

Setting the derivatives in (14) equal to zero yields a critical point $(\mathbf{p}^*(t), \phi^*(t))$ satisfying

$$\mathbf{p}^*(t) = \mathbf{b}_i(t), \quad (15a)$$

$$\phi_i^*(t) \in \left\{ \phi(t) \mid a_i(t) = \frac{1}{N} \right\}. \quad (15b)$$

Consider first the dual dynamics. The function $F(\mathbf{p}^*(t), \phi)$ is concave in ϕ in a neighborhood of ϕ^* [3]. Gradient ascent on this concave function drives the masses $a_i(t)$ toward the uniform allocation $\frac{1}{N}$, yielding the dual update

$$\dot{\phi}_i(t) = K_\phi \left(\frac{1}{N} - a_i(t) \right), \quad (16)$$

as also employed in [22].

The computation of the optimal barycenters is, in general, a nonconvex problem [28]. Formally, as noted in [22], an additional assumption is required to certify local convexity: if, for $\phi = \phi^*$, the Hessian $\nabla_{\mathbf{p}}^2 F(\mathbf{p}(t), \phi^*)$ is positive definite in a neighborhood of $\mathbf{p}^*(t)$, then the critical point is a strict local minimum. Nevertheless, gradient-based methods converge to local minimizers under standard regularity conditions. Global optimality is not claimed here; instead, following previous related works [28,22,13,12], the focus is on convergence to local minima that evolve with time. By (15), any such minimizer corresponds to agents located at the barycenters of their Laguerre cells [17].

To design dynamics that track the time-varying barycenters $\mathbf{b}(t)$, consider the candidate Lyapunov function

$$V = \frac{1}{2} \|\mathbf{p}(t)(t) - \mathbf{b}(t)\|_2^2.$$

Note that, for nondegenerate configurations of the Laguerre tessellation, the barycenters $\mathbf{b}_i(t)$ depend smoothly on the agents' positions [10,32,31]. However, topology changes in the Laguerre diagram, corresponding to degenerate configurations where three or more cell boundaries meet at a single point, can induce discontinuities in $\dot{\mathbf{b}}_i(t)$. Such degeneracies occur only on a set of measure zero in the configuration space [10]. Consequently, $\mathbf{b}(t)$ is absolutely continuous along trajectories, $\dot{\mathbf{b}}(t)$ exists almost everywhere, and solutions of (13) are understood in the Carathéodory sense [10,19].

Since both $\mathbf{p}(t)$ and $\mathbf{b}(t)$ are absolutely continuous, so is $V(t)$, and its time derivative satisfies, for almost all t ,

$$\dot{V} = (\mathbf{p}(t)(t) - \mathbf{b}(t))^\top (\dot{\mathbf{p}}(t) - \dot{\mathbf{b}}(t)).$$

Choosing

$$\dot{\mathbf{p}}_i(t) = -K_x (\mathbf{p}_i(t) - \mathbf{b}_i(t)) + \dot{\mathbf{b}}_i(t) \quad (17)$$

yields, almost everywhere,

$$\dot{V} = -K_x \|\mathbf{p}(t)(t) - \mathbf{b}(t)\|_2^2 = -2K_x V,$$

which implies exponential convergence of the tracking error to zero with rate $2K_x > 0$.

Hence, the coupled primal-dual system realizes a tracking scheme that follows the trajectory of instantaneous saddle points of the time-varying problem: the dual dynamics (16) perform gradient ascent to enforce equal-mass regions, while the primal dynamics (17) combine proportional feedback with feedforward compensation to track the evolving barycenters. \square

Equation (15) shows that, at optimality, the agents induce an *equal-mass* partition of the domain and coincide with the *barycenters* of their respective Laguerre regions. As the target density evolves, both the Laguerre cells and their barycenters change over time, giving rise to a naturally time-varying coverage problem.

The proposed dynamics in (13) steer each agent toward the time-varying reference $\mathbf{b}_i(t)$. Because this reference evolves in time, a pure gradient descent law would generally exhibit tracking lag. To eliminate this effect, a feedforward term is introduced that compensates for the motion of the barycenter, a standard technique in control theory and in minimum tracking problems [41,15]. The resulting control law combines proportional feedback with feedforward compensation, consistent with its Voronoi-based counterpart (see [28], Eq. III-3).

A key challenge in the proposed strategy is the derivation of $\dot{\mathbf{b}}_i(t)$. Applying the chain rule yields

$$\dot{\mathbf{b}}_i(t) = \frac{\partial \mathbf{b}_i}{\partial t} + \sum_{j \in \mathcal{N}_i} \left(\frac{\partial \mathbf{b}_i}{\partial \mathbf{p}_j} \dot{\mathbf{p}}_j + \frac{\partial \mathbf{b}_i}{\partial \phi_j} \dot{\phi}_j \right), \quad (18)$$

where \mathcal{N}_i denotes the set of Laguerre neighbors of agent i . This expression is generally cumbersome to find due to the time-varying integration domains [36]. In the one-dimensional case, however, a closed-form expression can be derived (see Sec. 5). More generally, the feedforward term can be approximated numerically via finite differences or by adopting the acceleration techniques in [16,28].

Remark 2 In numerical implementations, the isolated discontinuities arising from Laguerre topology changes have no practical effect since integrators operate on finite time steps. Standard explicit or implicit schemes applied to (13) produce trajectories that approximate the Carathéodory solutions without requiring special handling of these events.

Remark 3 In applications such as environmental monitoring or formation control, it is often reasonable to assume that $\partial_t \bar{\rho}(\mathbf{x}, t)$ is known. For instance, when the target density evolves according to a partial differential equation, a model-based estimate of $\partial_t \bar{\rho}(\mathbf{x}, t)$ can be obtained. Estimation errors in $\partial_t \bar{\rho}(\mathbf{x}, t)$ or $\mathbf{b}(t)$ can be viewed as bounded disturbances; the proportional feedback then yields bounded tracking errors and recovers exponential convergence in the ideal case. Numerical details on robustness with respect to uncertainty in $\partial_t \bar{\rho}(\mathbf{x}, t)$ are provided in Sec. 6.

Remark 4 The proposed framework clarifies the relationship between optimal transport and Voronoi-based strategies. In the optimal transport formulation, the objective is to approximate distributions rather than to optimize geometric coverage. Setting $K_\phi = 0$ with $\phi_i(0) = \phi$ for all i recovers the Voronoi-based strategy, whereas choosing $K_\phi > 0$ drives the partition toward equal-mass regions, thereby minimizing the Wasserstein distance. This metric provides a principled means of comparing continuous and discrete measures.

4.2 Numerical validation

The proposed strategy is validated in a two-dimensional domain where 7 agents track a Gaussian distribution $\mathcal{N}(\mathbf{m}(t), \Sigma)$ with linearly moving mean $\dot{\mathbf{m}}(t) = [v_{m,x}, v_{m,y}]$. The feedforward term $\mathbf{b}(t)$ is estimated online via a second-order sliding mode differentiator [29]:

$$\begin{cases} \dot{\mathbf{z}}_0 = -\lambda_1 |\mathbf{z}_0 - \mathbf{b}|^{1/2} \text{sign}(\mathbf{z}_0 - \mathbf{b}) + \mathbf{z}_1, \\ \dot{\mathbf{z}}_1 = -\lambda_2 \text{sign}(\mathbf{z}_0 - \mathbf{b}), \end{cases} \quad (19)$$

yielding $\dot{\mathbf{b}}(t) \approx \mathbf{z}_1(t)$. Parameters are reported in the Appendix. As shown in Fig. 2, the agents, initialized at random positions, rapidly reposition to cover the target and continue tracking it as the distribution moves across the domain, thereby minimizing the Wasserstein distance between the target and empirical measures (Figure 4a).

To further test the proposed strategy, a second experiment with 8 agents is presented in Fig. 3. The target density begins as a unimodal Gaussian with linearly varying mean and sinusoidally varying variance, causing the agents to contract and expand accordingly. After one period, the distribution splits into a bimodal Gaussian; the

agents then divide into two groups to cover the emerging modes and continue tracking as the modes separate. Throughout the experiment, the agents maintain coherent spatial arrangements while adapting to the evolving density. This experiment also demonstrates robustness to violations of Assumption 1. Although the target density is nondifferentiable at the switching instant $t = 3.14$ a.u., the proposed strategy continues to operate without degradation. Figure 4b shows the time evolution of the Wasserstein distance between the empirical and target measures. During the initial phase, the variance of the unimodal Gaussian varies sinusoidally, and the Wasserstein distance oscillates accordingly. At $t = 3.14$ a.u., the distribution becomes bimodal, introducing a point of nondifferentiability. After a brief transient, the Wasserstein error decreases and reaches a plateau as the variances remain constant.

Allowing the target density to vary over time also leads naturally to a formulation of formation control in probability space. This example is representative of how the proposed coverage control solution can be interpreted as a form of formation control by viewing the desired formation as a continuously evolving spatial density rather than a fixed geometric pattern. Instead of prescribing relative positions among agents, the formation is implicitly encoded by the target distribution, whose regions of high density define the shape and evolution of the formation. By driving agents to optimally approximate this density over time, the collective behavior naturally maintains coherent spatial arrangements that adapt smoothly to changes in the desired formation, environment, or task requirements.

Supplementary videos of the simulations are available at <https://shorturl.at/ublQV>.

5 One-dimensional case: Closed-form solution

Consider a one-dimensional domain $\Omega \subset \mathbb{R}$. In this setting, the feedforward term in (13) admits an explicit expression. As a consequence, a closed-form solution can be derived for the control input $\mathbf{u}(t) := \text{vec}(u_1(t), \dots, u_N(t))$.

Theorem 2 (Explicit dynamics in 1D) For $d = 1$, the feedforward term $\mathbf{b}(t)$ in (13) can be computed analytically, yielding the explicit dynamics

$$\begin{cases} \dot{\mathbf{p}}(t) = (\mathbb{I}_N - \mathbf{M}(t))^{-1} \left(-K_x (\mathbf{p}(t) - \mathbf{b}(t)) + \mathbf{q}(t) \right), \\ \dot{\phi}(t) = K_\phi \left(\frac{1}{N} - \mathbf{a}(t) \right), \end{cases} \quad (20)$$

where $K_x, K_\phi > 0$. The vector $\mathbf{q} \in \mathbb{R}^N$, defined in (31), is an inhomogeneous term whose i -th component depends on $\bar{\rho}(\mathbf{x}, t)$ and $\partial_t \bar{\rho}(\mathbf{x}, t)$ for $x \in \mathcal{V}_i$, as well as on (p_j, ϕ_j) for $j \in \{i-1, i, i+1\}$. The tridiagonal matrix $\mathbf{M} \in$

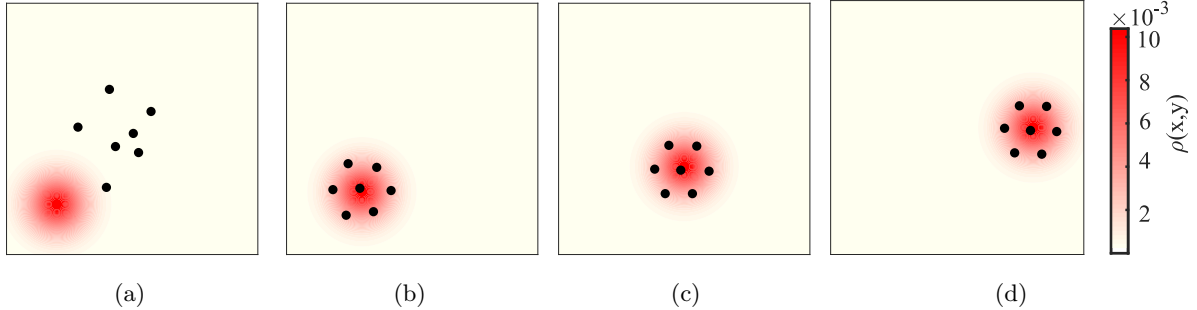


Fig. 2. Validation in two dimensions with 7 agents (black dots) covering a time-varying density at (a) $t = 0$, (b) $t = 0.5$, (c) $t = 1.5$, and (d) $t = 3$ a.u.

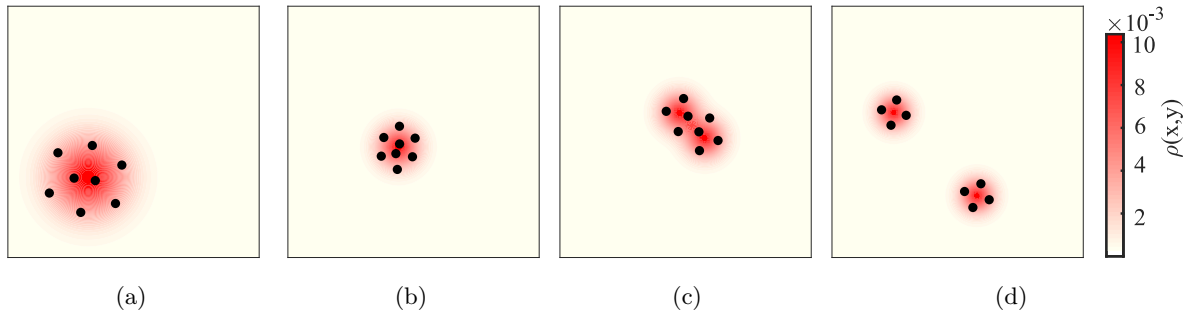


Fig. 3. Validation with 8 agents (black dots) covering a time-varying density at (a) $t = 1$, (b) $t = 2$, (c) $t = 4$, and (d) $t = 6$ a.u. The agents maintain formation as the density shrinks, expands, and splits into a bimodal distribution.

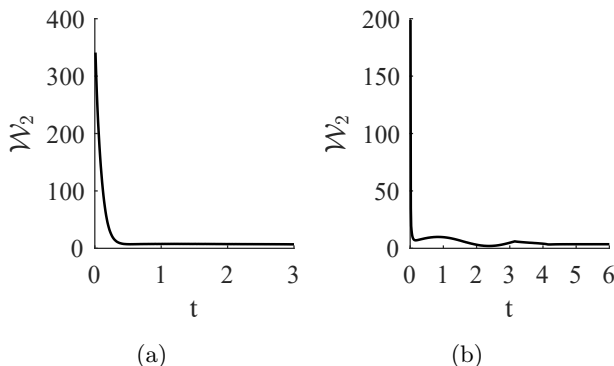


Fig. 4. Time evolution of the 2-Wasserstein distance between the empirical and target measures for (a) the first experiment, whose trajectories are reported in Figure 2, and (b) the second experiment, whose trajectories are reported in Figure 3.

$\mathbb{R}^{N \times N}$, defined in (32), captures the coupling induced by the motion of the Laguerre boundaries; its i -th row depends on $\bar{\rho}(\mathbf{x}, t)$ and (p_j, ϕ_j) for $j \in \{i-1, i, i+1\}$.

Proof. By Theorem 1, local asymptotic saddle-point tracking for Problem 9 is achieved by the dynamics in (13). In general, explicitly computing the feedforward term $\dot{\mathbf{b}}(t)$ is cumbersome, as it depends on moving Laguerre boundaries and therefore implicitly on $\dot{\mathbf{p}}$. In

one dimension, however, the structure simplifies significantly. Under Assumption 2, agents cannot overtake each other, and the neighborhood relations remain fixed. Each agent i has two neighbors, $i-1$ (left) and $i+1$ (right), except for the first and last agents, which have only one.¹ Consequently, the Laguerre cell of agent i is an interval $\mathcal{V}_i = [l_i, r_i]$.

Accordingly, the mass and barycenter of \mathcal{V}_i are given by

$$a_i = \int_{l_i}^{r_i} \bar{\rho}(x, t) dx, \quad b_i(t) = \frac{I_i(t)}{a_i(t)}, \quad (21)$$

where $I_i(t) := \int_{l_i}^{r_i} x \bar{\rho}(x, t) dx$. Differentiating b_i yields

$$\dot{b}_i = \frac{\dot{I}_i}{a_i} - \frac{b_i}{a_i} \dot{a}_i. \quad (22)$$

Applying Leibniz rule [11] gives

$$\dot{a}_i = \int_{l_i}^{r_i} \partial_t \bar{\rho}(x, t) dx + \bar{\rho}(r_i, t) \dot{r}_i - \bar{\rho}(l_i, t) \dot{l}_i, \quad (23)$$

$$\dot{I}_i = \int_{l_i}^{r_i} x \partial_t \bar{\rho}(x, t) dx + r_i \bar{\rho}(r_i, t) \dot{r}_i - l_i \bar{\rho}(l_i, t) \dot{l}_i. \quad (24)$$

¹ For simplicity, the domain Ω is assumed time invariant. Time-varying domains would introduce additional boundary terms for the first and last agents.

By construction, $r_i = l_{i+1}$ and $l_i = r_{i-1}$. From the definition of Laguerre cells (2), the boundary r_i satisfies

$$\frac{1}{2} \|p_i - r_i\|_2^2 - \phi_i = \frac{1}{2} \|p_{i+1} - r_i\|_2^2 - \phi_{i+1}. \quad (25)$$

from which we can isolate r_i

$$r_i = \frac{p_{i+1} + p_i}{2} + \frac{\phi_i - \phi_{i+1}}{p_{i+1} - p_i} = l_{i+1}. \quad (26)$$

Differentiating in time and using (13) gives:

$$\dot{r}_i = c_{i,i} u_i + c_{i,i+1} u_{i+1} + \tilde{q}_i = \dot{l}_{i+1}, \quad (27)$$

where the coefficients are defined as follows

$$c_{i,i} := \frac{1}{2} + \frac{\phi_i - \phi_{i+1}}{(p_{i+1} - p_i)^2}, \quad (28)$$

$$c_{i,i+1} := \frac{1}{2} - \frac{\phi_i - \phi_{i+1}}{(p_{i+1} - p_i)^2}, \quad (29)$$

$$\tilde{q}_i := \frac{K_\phi(a_{i+1} - a_i)}{p_{i+1} - p_i}. \quad (30)$$

Substituting (27) into (22)–(23) yields

$$\begin{aligned} \dot{b}_i &= \frac{1}{a_i} \int_{l_i}^{r_i} (x - b_i) \partial_t \bar{\rho}(x, t) dx + \delta_i^r \tilde{q}_i - \delta_i^l \tilde{q}_{i-1} + \\ &\quad - \delta_i^l c_{i-1,i-1} u_{i-1} + \delta_i^r c_{i,i+1} u_{i+1} + (\delta_i^r c_{i,i} - \delta_i^l c_{i-1,i}) u_i, \end{aligned}$$

where

$$\begin{aligned} \delta_i^r &:= (r_i - b_i) \bar{\rho}(r_i) / a_i, \\ \delta_i^l &:= (l_i - b_i) \bar{\rho}(l_i) / a_i. \end{aligned}$$

Next, define $\mathbf{q} \in \mathbb{R}^N$ with components

$$q_i := \frac{1}{a_i} \int_{l_i}^{r_i} (x - b_i) \partial_t \bar{\rho}(x, t) dx + \delta_i^r \tilde{q}_i - \delta_i^l \tilde{q}_{i-1}, \quad (31)$$

and the tridiagonal matrix $\mathbf{M} \in \mathbb{R}^{N \times N}$ with entries

$$\begin{cases} m_{i,i-1} := -\delta_i^l c_{i-1,i-1}, \\ m_{i,i} := \delta_i^r c_{i,i} - \delta_i^l c_{i-1,i}, \\ m_{i,i+1} := \delta_i^r c_{i,i+1}. \end{cases} \quad (32)$$

Then the control input satisfies

$$\mathbf{u} = -K_x(\mathbf{p} - \mathbf{b}) + \mathbf{M}\mathbf{u} + \mathbf{q}, \quad (33)$$

where the last two terms correspond to $\dot{\mathbf{b}}(t)$. Provided that $(\mathbb{I}_N - \mathbf{M})$ is invertible (see Remark 5), isolating \mathbf{u} yields the explicit solution (20). \square

Remark 5 The entries of \mathbf{M} depend on boundary density values and interagent distances. Under Assumption 1, these quantities remain bounded and $\|\mathbf{M}\|_2 < 1$ typically holds, ensuring invertibility of $(\mathbb{I}_N - \mathbf{M})$ via the Neumann series [21]. Physically, \mathbf{M} encodes the coupling induced by boundary motion; when this effect is negligible, (20) reduces to decoupled tracking dynamics.

Remark 6 In one dimension, Assumption 2 prevents agents from overtaking one another, so the ordering of agents remains fixed and topology changes in the Laguerre diagram cannot occur. Consequently, the barycenters $\mathbf{b}_i(t)$ are differentiable globally in time, and the regularity considerations of Remark 2 are automatically satisfied.

Moreover, for the one-dimensional case, a sufficient condition for convexity of the objective function with respect to $\mathbf{p}(t)$ is provided in [22]:

$$\begin{aligned} h_{\max} &:= \max_i 2N \sum_{j \in \{i-1, i+1\}} \left| \frac{x_i^* - x_j^*}{4} + \frac{\phi_i^* - \phi_j^*}{x_i^* - x_j^*} \right| \\ &\quad \left(\frac{1}{2} + 2 \frac{|\phi_i^* - \phi_j^*|}{(x_i^* - x_j^*)^2} \right) \bar{\rho} \left(\frac{x_i^* + x_j^*}{4} - \frac{\phi_i^* - \phi_j^*}{x_i^* - x_j^*}, \cdot \right) < 1. \end{aligned} \quad (34)$$

This condition does not involve time derivatives of the Hessian; hence, if it holds uniformly in time, it extends directly to the time-varying setting. Convexity in $\mathbf{p}(t)$ combined with concavity in $\phi(t)$ yields a convex-concave saddle point, ensuring that gradient descent ascent converges to the local optimum [22].

5.1 Numerical validation

The closed-form solution (20) is validated across three scenarios in a one-dimensional domain.

In the first scenario, a Gaussian target distribution with linearly varying mean is considered: $\bar{\rho}(\mathbf{x}, t) = \mathcal{N}(m(t), \sigma)$ with $\dot{m}(t) = v_m$ and $m(0) = m_0$. As shown in Fig. 5a, the agents successfully track the moving Gaussian. The first and last agents move toward the tails while the central agents remain closer together, consistent with the equal-mass requirement $a_i = 1/N$. After a short transient, the agents exhibit no tracking lag and the Wasserstein distance remains minimal (Fig. 5d, solid black line).

In the second scenario, both the mean and variance vary sinusoidally: $\bar{\rho}(\mathbf{x}, t) = \mathcal{N}(m(t), \sigma(t))$ with $\dot{m}(t) = v_m \sin(t)$ and $\dot{\sigma}(t) = v_\sigma \sin(t)$. The agents compress when the variance decreases and spread out when it increases, tracking the oscillating mean without lag (Fig. 5b). The Wasserstein distance oscillates in response to the varying variance (Fig. 5e, solid black line).

In the third scenario, a bimodal distribution $\bar{\rho}(\mathbf{x}, t) = 0.5\mathcal{N}(m_1(t), \sigma) + 0.5\mathcal{N}(m_2(t), \sigma)$ with $\dot{m}_i = v_{m,i}$ is considered. The agents split into two groups near the peaks, accurately reproducing the target (Fig. 5c), and the Wasserstein distance converges to a constant value (Fig. 5f).

Supplementary videos of the simulations are available at <https://shorturl.at/ublQV>.

These experiments validate the one-dimensional solution. Section 6 provides a quantitative comparison with alternative strategies, demonstrating the necessity of the feedforward term and the superior performance relative to Voronoi-based approaches.

5.2 Distributed implementation

The Neumann series described in Remark 5 also suggests a distributed approximation. Truncating the series at order k yields $(\mathbb{I}_N - \mathbf{M})^{-1} \approx \sum_{j=0}^k \mathbf{M}^j$, and since \mathbf{M} is tridiagonal, row i of \mathbf{M}^j depends only on agents within index distance j of agent i . Each agent can therefore compute this approximation through k rounds of nearest neighbor communication, leading to a distributed implementation analogous to that in [28].

To illustrate the effectiveness of this approach, we include a representative simulation example showing that the truncated approximation achieves satisfactory performance in practice. We reconsider the first scenario described in Section 5.1 and approximate $(\mathbb{I}_N - \mathbf{M})^{-1} \approx \mathbb{I}_N + \mathbf{M}$, that is, we take $k = 1$, while keeping the gains fixed as in the centralized case. Under this approximation, each agent only needs to communicate with its left and right neighbors.

Figure 6 shows that the agents still track the time-varying density effectively despite the strong truncation and limited communication. The performance degrades slightly compared to the centralized solution, with a slower response to variations in the target distribution that produces small overshoots in the trajectories. Nevertheless, the agents recover quickly without exhibiting significant lag, achieving nearly perfect tracking and a Wasserstein error that converges to a plateau comparable to that of the centralized case.

A more detailed theoretical and numerical analysis of this approximation is left for future work.

6 Comparative analysis

The proposed strategy (TV-OT) is benchmarked against two baselines: static optimal transport coverage control (OTCC) [22] and time-varying Voronoi-based control (TV-V) [28]. Simulation parameters are summarized in

Table A.2, and the Wasserstein distance serves as the primary performance metric. For a fair comparison, since TV-OT explicitly minimizes this metric, the Kullback-Leibler divergence $D_{KL}(\bar{\rho} \parallel \hat{\rho})$ is also computed, where $\hat{\rho}$ is estimated via kernel density estimation with Silverman bandwidth selection [9,6]. The three scenarios from Sec. 5.1 are considered, and for each the convexity condition (34) is verified, with $h_{\max} = 2.13 \times 10^{-20}$, 1.61×10^{-1} , and 3.19×10^{-4} , respectively, all less than 1. Table 1 reports the resulting metrics. Across all scenarios, TV-OT achieves substantially lower Wasserstein distance than both baselines, and without the feedforward term the agents lag behind the moving density, leading to significantly larger errors. These performance gaps are also reflected in the KL divergence.

Figure 5d–f confirms that the Wasserstein error remains lower throughout each experiment for TV-OT compared to both OTCC and TV-V. The Voronoi-based approach converges to a steady error slightly higher than TV-OT, since the latter directly minimizes the approximation error. Numerically approximating $\mathbf{b}(t)$ via finite differences yields Wasserstein errors close to the analytical solution, though with increased sensitivity to gain tuning and numerical approximations, as evident at $t = 18$ a.u. in Fig. 5f. The benefit of feedforward compensation is further quantified in Fig. 7, which compares TV-OT and OTCC for varying density drift velocity $v_m \in [0.5, 4]$ and gain $K_x \in [0.5, 4]$. Without feedforward, acceptable accuracy requires large gains and slow drift; otherwise, persistent lag produces substantial steady-state error. With feedforward, TV-OT achieves significantly smaller errors across the entire parameter range.

Robustness to uncertainty in $\partial_t \bar{\rho}(\mathbf{x}, t)$ is evaluated in Fig. 8, where perturbations of $\pm 20\%$ are introduced in the estimated drift velocity for target velocities $\dot{m} \in \{1, 5, 10\}$. Increasing K_x reduces sensitivity to estimation errors, and tracking error remains bounded for a suitable range of parameters; as expected, faster references under uncertainty require higher gains. Finally, scalability is examined by varying $N \in [10, 100]$. Figure 9 shows that the squared Wasserstein error decays approximately as $1/N$, consistent with optimal quantization theory [33]. In summary, TV-OT achieves accurate tracking of time-varying densities, outperforming TV-V due to its optimal transport formulation and OTCC due to the feedforward term enabling dynamic tracking.

7 Conclusions

This paper addressed coverage control for multi-agent systems tracking time-varying densities within an optimal transport framework. By formulating the problem as a time-dependent semi-discrete optimal transport task, a principled approach was developed that handles continuously evolving target densities while preserving

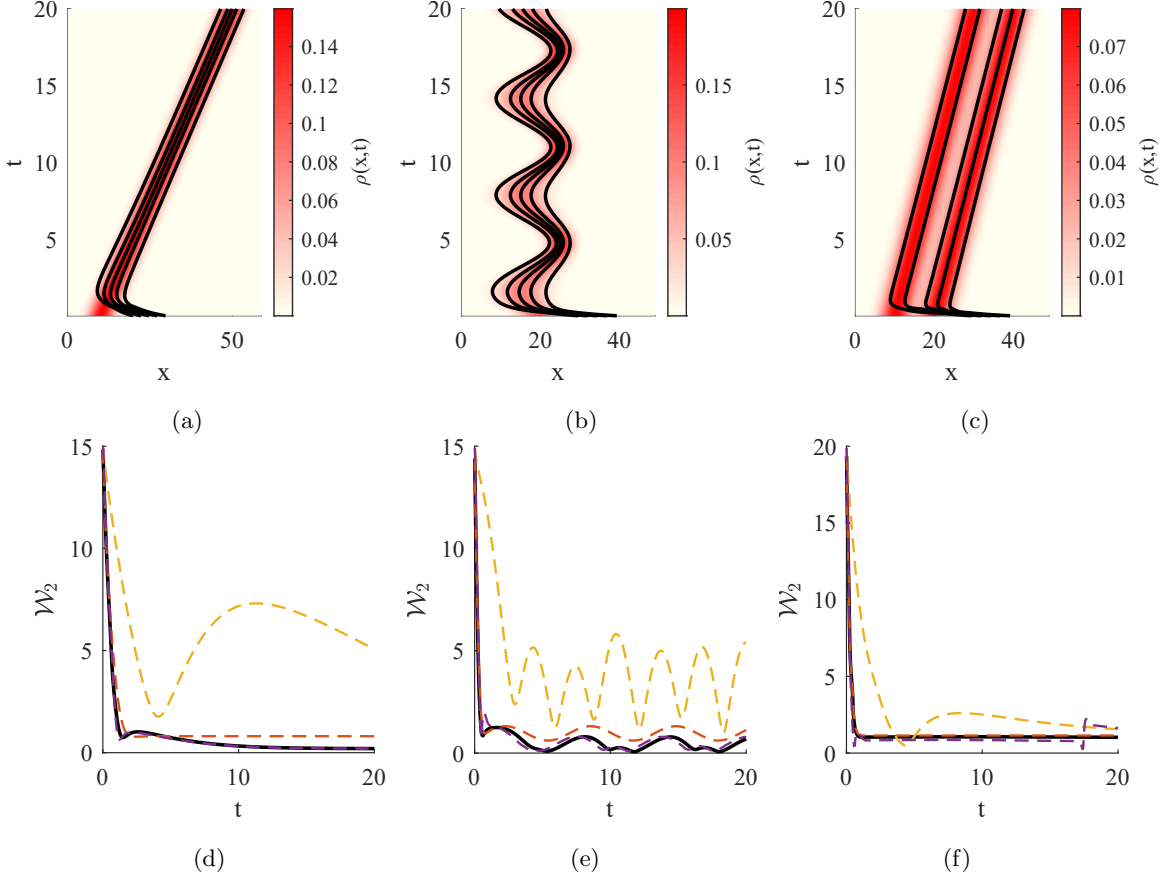


Fig. 5. Validation of the proposed method in one-dimensional domains with 5 agents. The evolution of densities (background color from white to red) and agent trajectories (solid black lines) is shown in space (x-axis) and time (y-axis). (a) First scenario: agents track a Gaussian distribution whose mean varies linearly over time; (b) Second scenario: both the mean and variance of the Gaussian distribution vary sinusoidally over time; (c) Third scenario: the mean of a multimodal Gaussian distribution varies linearly over time. Panels (d)–(f) show the Wasserstein distances over time between the empirical and target distributions of the three scenarios, respectively, for the proposed strategy (black solid line), for the case without the feedforward term ([22], yellow dotted line), for the Voronoi-based solution (red dotted line), and when the feedforward term is computed numerically (purple dotted line).

Scenario	Method	\mathcal{W}_2	D_{KL}
1	TV-OT	0.2003	0.0250
	TV-V	0.8052	0.1507
	OTCC	5.1054	0.7122
2	TV-OT	0.6933	0.0697
	TV-V	1.1233	0.1316
	OTCC	5.3996	0.5307
3	TV-OT	1.0289	0.3025
	TV-V	1.1464	0.3096
	OTCC	1.5604	0.3239

Table 1
Performance metrics for TV-OT, TV-V [28], and OTCC [22] across the three scenarios of Sec. 5.1.

the feedback and feedforward structure of classical coverage methods. This formulation naturally generalizes

centroidal Voronoi-based approaches and offers a principled method to approach formation control problems in the probability space.

Coupled dynamics for the agent positions and the dual variables defining the Laguerre tessellation were derived. The resulting control laws steer agents toward the time-varying barycenters of their Laguerre cells, while the dual variables maintain mass balance as the target density evolves. A closed-form expression for the control law in one dimension was presented, and extensive validation demonstrated superior performance compared to Voronoi-based and quasi-static optimal transport-based algorithms. Robustness to estimation errors and scaling laws were also analyzed.

Future work will focus on incorporating practical constraints such as limited sensing, communication delays, and obstacles. Decentralized implementations will be

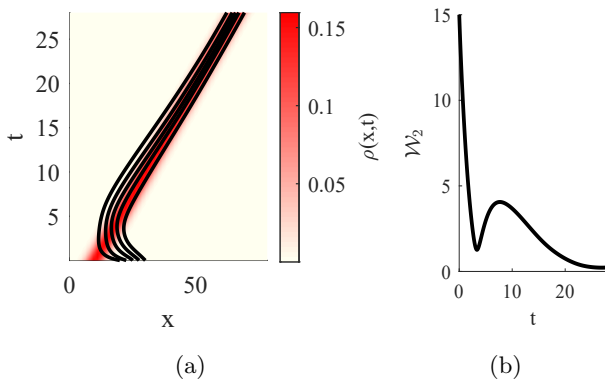


Fig. 6. Validation of the proposed method in one-dimensional domains with 5 agents in a distributed fashion, assuming each agent can only communicate with its closest neighbors to the left and right. (a) The evolution of densities (background color from white to red) and agent trajectories (solid black lines) is shown in space (x-axis) and time (y-axis). Panel (b) show the Wasserstein distances over time between the empirical and target distributions.

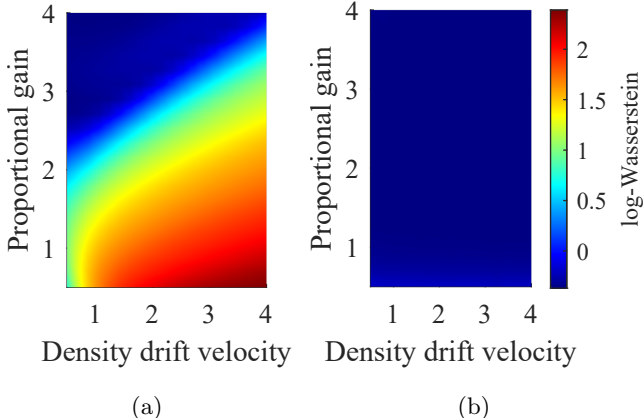


Fig. 7. Wasserstein error (log scale) as a function of density drift velocity (x-axis) and gain K_x (y-axis) for (a) OTCC without feedforward and (b) the proposed TV-OT strategy.

further investigated via approximations similar to those in [28], and entropy-regularized formulations offer a promising direction for improved computational efficiency [14].

Acknowledgements

The authors wish to thank Davide Salzano, University of Naples Federico II, and Giovanni Russo, University of Salerno, for the useful discussions. During the preparation of this manuscript, the authors used AI-based tools to improve readability and language. The authors have reviewed and edited the output and take full responsibility for the content of this publication.

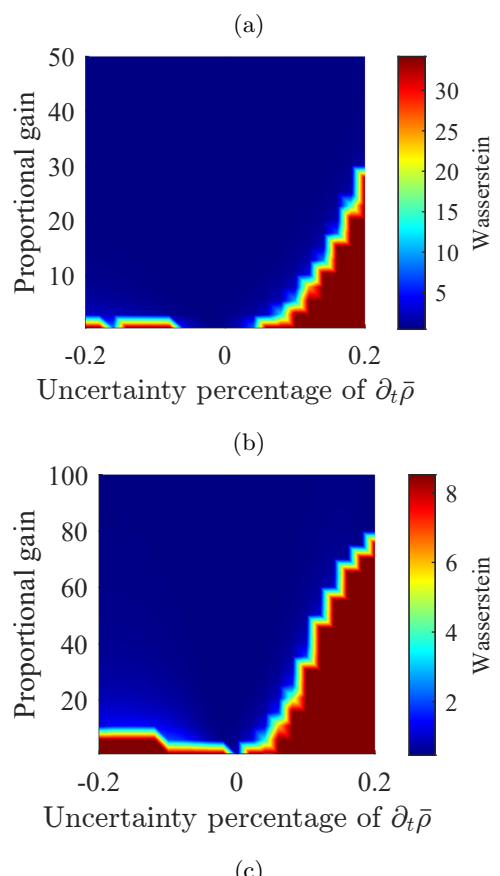
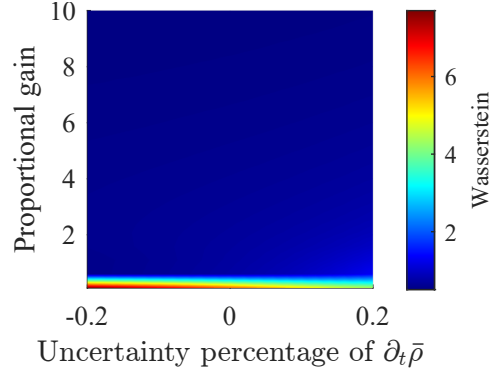


Fig. 8. Robustness analysis showing Wasserstein error for varying estimation errors in $\partial_t \bar{\rho}(\mathbf{x}, t)$ (x-axis) and gain K_x (y-axis). The target mean velocity is (a) 5, (b) 5, and (c) 10 a.u.

A Simulation parameters

Here, we report the parameters used in the experiments.

References

[1] Jason M Altschuler, Jonathan Niles-Weed, and Austin J Stromme. Asymptotics for semidiscrete entropic optimal transport. *SIAM Journal on Mathematical Analysis*, 54(2):1718–1741, 2022.

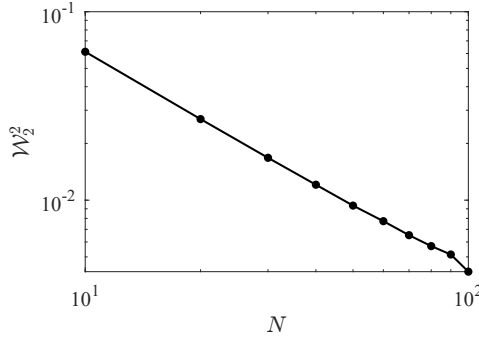


Fig. 9. Scaling analysis showing the squared Wasserstein error at final time versus number of agents N (log-log scale). The slope of approximately -1.08 indicates $\mathcal{W}_2^2 \sim 1/N$.

Ω	$[0, 50]^2$	λ_1	9
Δt	0.01	λ_2	10
Δx	0.5	m_0	[10, 10]
K_x	20	Σ	diag(15, 15)
K_ϕ	10	\dot{m}	[10, 5]

Table A.1
Parameters used in the experiment for Sec. 4.2.

	Exp 1	Exp 2	Exp 3
Ω	[0, 60]	[0, 50]	[0, 50]
K_x	2	5	5
K_ϕ	1	2.5	1
Δt	0.01	0.01	0.01
Δx	0.012	0.01	0.01
m_0	10	20	10, 20
σ_0	2.5	3	2, 2
\dot{m}	2	-5	1, 1
$\dot{\sigma}$	0	1	0, 0

Table A.2
Parameters used in the experiment for Sec. 5.1 and 6.

- [2] Franz Aurenhammer. Power diagrams: properties, algorithms and applications. *SIAM journal on computing*, 16(1):78–96, 1987.
- [3] Franz Aurenhammer, Friedrich Hoffmann, and Boris Aronov. Minkowski-type theorems and least-squares clustering. *Algorithmica*, 20(1):61–76, 1998.
- [4] Saptarshi Bandyopadhyay, Soon-Jo Chung, and Fred Y Hadaegh. Probabilistic swarm guidance using optimal transport. In *IEEE Conference on Control Applications*, pages 498–505, 2014.
- [5] Jean-David Benamou and Yann Brenier. A computational fluid mechanics solution to the monge-kantorovich mass transfer problem. *Numerische Mathematik*, 84(3):375–393, 2000.
- [6] Silverman Bernard W. *Density Estimation for Statistics and Data Analysis*. Chapman & Hall/CRC, 1986.
- [7] David P Bourne and Steven M Roper. Centroidal power diagrams, lloyd's algorithm, and applications to optimal

location problems. *SIAM Journal on Numerical Analysis*, 53(6):2545–2569, 2015.

- [8] Francesco Bullo, Jorge Cortés, and Sonia Martínez. *Distributed control of robotic networks: a mathematical approach to motion coordination algorithms*. Princeton University Press, 2009.
- [9] Yen-Chi Chen. A tutorial on kernel density estimation and recent advances. *Biostatistics & Epidemiology*, 1(1):161–187, 2017.
- [10] Jorge Cortés. Discontinuous dynamical systems. *IEEE Control Systems Magazine*, 28(3):36–73, 2008.
- [11] Jorge Cortes, Sonia Martínez, and Francesco Bullo. Spatially-distributed coverage optimization and control with limited-range interactions. *ESAIM: Control, Optimisation and Calculus of Variations*, 11(4):691–719, 2005.
- [12] Jorge Cortes, Sonia Martínez, Timur Karatas, and Francesco Bullo. Coverage control for mobile sensing networks: variation on a theme. *Mediterranean Conference Control Automatic*, 2002.
- [13] Jorge Cortes, Sonia Martínez, Timur Karatas, and Francesco Bullo. Coverage control for mobile sensing networks. *IEEE Transactions on robotics and Automation*, 20(2):243–255, 2004.
- [14] Marco Cuturi. Sinkhorn distances: Lightspeed computation of optimal transport. *Advances in neural information processing systems*, 26, 2013.
- [15] Alexander Davydov, Veronica Centorrino, Anand Gokhale, Giovanni Russo, and Francesco Bullo. Time-varying convex optimization: A contraction and equilibrium tracking approach. *IEEE Transactions on Automatic Control*, 70(11):7446–7460, 2025.
- [16] Qiang Du and Maria Emelianenko. Acceleration schemes for computing centroidal voronoi tessellations. *Numerical linear algebra with applications*, 13(2-3):173–192, 2006.
- [17] Qiang Du, Maria Emelianenko, and Lili Ju. Convergence of the lloyd algorithm for computing centroidal voronoi tessellations. *SIAM journal on numerical analysis*, 44(1):102–119, 2006.
- [18] Qiang Du, Vance Faber, and Max Gunzburger. Centroidal voronoi tessellations: Applications and algorithms. *SIAM review*, 41(4):637–676, 1999.
- [19] Aleksei F. Filippov. *Differential Equations with Discontinuous Righthand Sides*, volume 18 of *Mathematics and Its Applications*. Kluwer Academic Publishers, 1988.
- [20] Greg Foderaro, Pingping Zhu, Hongchuan Wei, Thomas A Wettergren, and Silvia Ferrari. Distributed optimal control of sensor networks for dynamic target tracking. *IEEE Transactions on Control of Network Systems*, 5(1):142–153, 2016.
- [21] Roger A. Horn and Charles R. Johnson. *Matrix Analysis*. Cambridge University Press, 2012.
- [22] Daisuke Inoue, Yuji Ito, and Hiroaki Yoshida. Optimal transport-based coverage control for swarm robot systems: Generalization of the voronoi tessellation-based method. *IEEE Control Systems Letters*, 5(4):1483–1488, 2020.
- [23] Leonid V Kantorovich. On the translocation of masses. In *Dokl. Akad. Nauk. USSR (NS)*, volume 37, pages 199–201, 1942.
- [24] Joshua Keene, Chris Manzie, Peter M Dower, and Airlie Chapman. Towards coverage control with jointly time-varying coverage regions and density functions. In *IEEE 63rd Conference on Decision and Control*, pages 7637–7643, 2024.

[25] Vishaal Krishnan and Sonia Martínez. A multiscale analysis of multi-agent coverage control algorithms. *Automatica*, 145:110516, 2022.

[26] Vishaal Krishnan and Sonia Martínez. Distributed online optimization for multi-agent optimal transport. *Automatica*, 170:111880, 2024.

[27] Seung Joon Lee, Yancy Diaz-Mercado, and Magnus Egerstedt. Dynamic coverage control in unicycle multi-robot networks under anisotropic sensing. *Frontiers in Robotics and AI*, 2:3, 2015.

[28] Sung G Lee, Yancy Diaz-Mercado, and Magnus Egerstedt. Multirobot control using time-varying density functions. *IEEE Transactions on robotics*, 31(2):489–493, 2015.

[29] Arie Levant. Higher-order sliding modes, differentiation and output-feedback control. *International journal of Control*, 76(9-10):924–941, 2003.

[30] Ruoyu Lin, Soobum Kim, and Magnus Egerstedt. Heterogeneous collaborative pursuit via coverage control driven by fokker-planck equations. *IEEE Transactions on Robotics*, 41:3649–3668, 2025.

[31] Yang Liu, Wenping Wang, Bruno Lévy, Feng Sun, Dong-Ming Yan, Lin Lu, and Chenglei Yang. On centroidal voronoi tessellation—energy smoothness and fast computation. *ACM Transactions on Graphics (ToG)*, 28(4):1–17, 2009.

[32] Quentin Mérigot. A multiscale approach to optimal transport. *Computer Graphics Forum*, 30(5):1583–1592, 2011.

[33] Quentin Mérigot and Jean-Marie Mirebeau. Minimal geodesics along volume-preserving maps, through semidiscrete optimal transport. *SIAM Journal on Numerical Analysis*, 54(6):3465–3492, 2016.

[34] Gaspard Monge. Mémoire sur la théorie des déblais et des remblais. *Mem. Math. Phys. Acad. Royale Sci.*, pages 666–704, 1781.

[35] Gabriel Peyré, Marco Cuturi, et al. Computational optimal transport: With applications to data science. *Foundations and Trends® in Machine Learning*, 11(5-6):355–607, 2019.

[36] Luciano CA Pimenta, Mac Schwager, Quentin Lindsey, Vijay Kumar, Daniela Rus, Renato C Mesquita, and Guilherme AS Pereira. Simultaneous coverage and tracking (scat) of moving targets with robot networks. In *Algorithmic Foundation of Robotics VIII: Selected Contributions of the Eight International Workshop on the Algorithmic Foundations of Robotics*, pages 85–99. Springer, 2009.

[37] Mac Schwager, Daniela Rus, and Jean-Jacques Slotine. Decentralized, adaptive coverage control for networked robots. *The International Journal of Robotics Research*, 28(3):357–375, 2009.

[38] Mac Schwager, Michael P Vitus, Samantha Powers, Daniela Rus, and Claire J Tomlin. Robust adaptive coverage control for robotic sensor networks. *IEEE Transactions on Control of Network Systems*, 4(3):462–476, 2015.

[39] Bahar Taşkesen, Soroosh Shafieezadeh-Abadeh, and Daniel Kuhn. Semi-discrete optimal transport: Hardness, regularization and numerical solution. *Mathematical Programming*, 199(1):1033–1106, 2023.

[40] Cédric Villani et al. *Optimal transport: old and new*, volume 338. Springer, 2008.

[41] Y Zhao and MNS Swamy. A novel technique for tracking time-varying minimum and its applications. In *Conference Proceedings. IEEE Canadian Conference on Electrical and Computer Engineering (Cat. No. 98TH8341)*, volume 2, pages 910–913. IEEE, 1998.